Available online at www.sciencedirect.com
SCIENCE DIRECT®
Physics Letters A 336 (2005) 245–252
PHYSICS LETTERS A
www.elsevier.com/locate/pla

Discontinuity effect on the phonon transmission and thermal conductance in a dielectric quantum waveguide

Wei-Qing Huang [a,b], Ke-Qiu Chen [b,*], Z. Shuai [b,*], Lingling Wang [a], Wangyu Hu [a]

[a] *Department of Applied Physics, Hunan University, Changsha 410082, China*
[b] *Laboratory of Organic Solids, Center for Molecular Sciences, Institute of Chemistry, Chinese Academy of Sciences, 100080 Beijing, China*

Received 13 December 2004; accepted 27 December 2004

Available online 13 January 2005

Communicated by V.M. Agranovich

Abstract

We investigate the effect of the discontinuity on the acoustic phonon transmission and thermal conductance in a dielectric quantum waveguide at low temperatures by using the scattering matrix method. It is found that the total transmission coefficient versus the reduced frequency exhibits strong resonant behavior. The reduced thermal conductance exhibits a universal quantization at low enough temperatures, independent of the parameters of structure, and decreases below the ideal universal value for the low temperatures due to the strong scattering of phonons by the discontinuity. A comparison between different discontinuity structures is made. Our results show that the transmission coefficient and thermal conductance sensitively depend on the geometric configurations.

PACS: 63.22.+m; 73.23.Ad; 44.10.+i

1. Introduction

Thermal transport in nanoscale systems whose dimensions are comparable to or less than the wavelength of thermal phonons has attracted intensive attention during the last decade [1,2]. The diffusive phonon transport and thermal conductivity in various kinds of nanostructures, such as thin film [3,4], quantum well [5], superlattices [6,7], nanowires [8–10], one-dimensional glass [11], and nanotube [12–14] have been studied experimentally and theoretically. In recent years, significant progress has also been made in the understanding of the ballistic phonon transport in these systems at low temperatures. One of the most striking phenomena is that theoretical analyses of phonon transport predict a thermal conductance K that is independent of the geometry and nature of the material [15], and a universal value $K/T = \pi^2 k_B^2/3h$ at low enough temperatures [16,17]. These theoretical

* Corresponding authors.
E-mail addresses: keqiuchen@iccas.ac.cn (K.-Q. Chen), zgshuai@iccas.ac.cn (Z. Shuai).

0375-9601/$ – see front matter
doi:10.1016/j.physleta.2004.12.089

predications was then confirmed by Schwab et al. [18] in tiny suspended silicon nitride devices. Their elegant experiment also showed a decrease in the thermal conductance below the universal value in low temperature except for the universality of ballistic phonon transport. This was also explained by Santamore et al. in terms of the scattering of thermal phonons of surface roughness [19,20]. These works motivate further investigations of the ballistic thermal conductance in a thin plate, [21] four-terminal mesoscopic dielectric system [22], single-walled boron nitride nanotubes [23], a curved wire [24], carbon nanotubes [25], and so on.

More recently, Li and co-workers calculated the phonon transmission and thermal conductance in the quantum waveguide structures with use of the scattering matrix method [26–28]. Some interesting features are revealed, such as acoustic phonon mode splitting behavior and the noninteger quantized thermal conductance in an asymmetric y-branch three terminal junction [28], and phonon transmission and thermal conductance can be controlled by adjusting the parameters of the stub in a T-shaped waveguide structure [27]. It is also found that the transmission coefficient is of quantum characteristic in the wide-narrow-wide (WNW) quantum structure [26]. In fact, all these structures can be classified as discontinuity quantum waveguides. In the present Letter, we use a scalar model for the elastic waves [15,19,21,22] to investigate the phonon transmission and thermal conductance in a narrow-wide-narrow (NWN) quantum waveguide structure, schematically shown in Fig. 1. Here the discontinuity in the waveguide structure is only in the y direction so that the solution may be assumed to be independent of the z coordinate without any loss of generality. We also employ the scattering matrix method [29–31], which is an effective method to calculate the electronic or phonon transport in one-dimensional or quasi-one-dimensional mesoscopic systems. Our results show some interesting properties of the phonon transmission and thermal conductance in such a discontinuity structure, which is very different from those presented in the other discontinuity quantum waveguides [26,27].

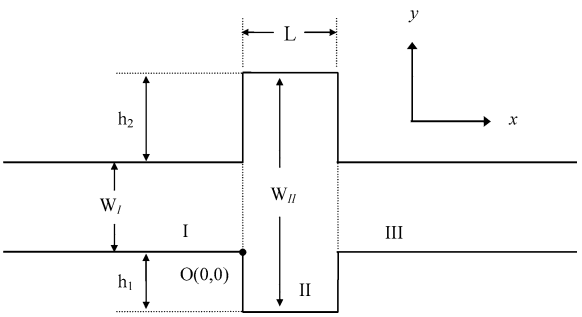

Fig. 1. Two semi-infinite quantum wires I and II with transverse dimension W_{I} are connected by the cavity with length L. The transverse dimension of the cavity is W_{II}. The heights of the lower and upper stubs denote as h_1 and h_2, respectively.

In the next section, we present a brief description of the model and the necessary formulae used in calculations. In Section 3, the results of the numerical calculations are given with analyses. Finally, we summarize our results in Section 4.

2. Model and formalism

The geometry we consider is a narrow–wide–narrow (NWN) wave-guide-like structure, as sketched in Fig. 1. The main part of the structure is a uniform waveguide with transverse dimension W_I. The region II consists of three parts: a segment of the main waveguide, the lower, and upper stubs with longitudinal dimension L. The heights of the lower and upper stubs are h_1 and h_2, respectively. We assume that the temperatures in regions I and III are T_1 and T_3, respectively; and the temperature difference δT ($\delta T = T_1 - T_3 > 0$) is very small, i.e., $\delta T \ll T_1, T_3$ [17]. So the mean temperature T [$T = (T_1 + T_3)/2$] can be adopted as the temperature of regions I and III in following calculations. In the general three-dimensional case, if the three regions have the same thickness, which is small with respect to the other two dimensions and also to the wavelength or the coherence length of the elastic waves, there is no mixing of the z modes and a two-dimensional calculation is adequate [15,19,21,22]. Considering imperfect contact at the regions I and III, the expression for the thermal conductance K at temperature T is given by [15–17]

$$K = \frac{\hbar^2}{k_B T^2} \sum_m \frac{1}{2\pi} \int_{\omega_m}^{\infty} \tau_m(\omega) \frac{\omega^2 e^{\beta\hbar\omega}}{(e^{\beta\hbar\omega} - 1)^2} d\omega. \qquad (1)$$

Here $\tau_m(\omega)$ is the transmission coefficient from mode m of region I at frequency ω across all the interfaces

into the modes of region III; ω_m is the cutoff frequency of the mth mode; $\beta = 1/(k_B T)$, k_B is the Boltzman constant, T is the temperature; and $\hbar$ is the Planck's constant. Here the integration is over the frequency ω of the modes m propagating in the structure. The effect of scattering is introduced through the transmission coefficient $\tau_m(\omega)$, which for continuity case (i.e., $h_1 = h_2 = 0$), $\tau_m(\omega) = 1$. The essential issue to calculate the thermal conductance is then to calculate the transmission coefficient, $\tau_m(\omega)$.

As discussed in the introduction, we use the scalar model for the elastic wave, and model a thin geometry at low temperature so that a two-dimensional calculation is adequate. Considering the horizontally polarized wave (SH) (polarized along the z direction) propagating in the x direction, the displacement field u satisfies the wave equation

$$\frac{\partial^2 u}{\partial t^2} - v_{\mathrm{SH}}^2 \nabla^2 u = 0, \tag{2}$$

where the SH wave velocity v_{SH} is related to the mass density ρ and elastic stiffness constant C_{44}

$$v_{\mathrm{SH}} = \sqrt{C_{44}/\rho}. \tag{3}$$

The stress-free boundary conditions apply at the edges

$$\hat{n} \cdot \nabla u = 0, \tag{4}$$

with $\hat{n}$ being the edge normal. The phonon displacement field equations in region ζ (regions I, II, and III) can then be written in the form

$$u^{\zeta}(x, y) = \sum_{m=0}^{N} \left[g_m^{\zeta} e^{i k_m^{\zeta}(x - x_{\zeta})} + h_m^{\zeta} e^{-i k_m^{\zeta}(x - x_{\zeta})} \right] \phi_m^{\zeta}(y), \tag{5}$$

where x_{ζ} is the reference coordinate along the x direction for region ζ. g_m and h_m are constants to be determined by matching the boundary conditions. $\phi_m^{\zeta}(y)$ [ζ: I, II, and III] represents the orthogonal transverse mode m in region ζ

$$\phi_m^{\zeta}(y) = \begin{cases} \sqrt{\frac{2}{W_{\zeta}}} \cos \frac{m\pi}{W_{\zeta}} y & (m \neq 0), \\ \sqrt{\frac{1}{W_{\zeta}}} & (m = 0); \end{cases} \tag{6}$$

k_m^{ζ} can be expressed in terms of incident phonon frequency ω, the SH wave velocity v_{SH}^{ζ}, and the transverse dimension W_{ζ} of region ζ by the energy conservation condition

$$k_m^{\zeta\,2} = \frac{\omega^2}{v_{\mathrm{SH}}^{\zeta\,2}} - \frac{m^2 \pi^2}{W_{\zeta}^2}. \tag{7}$$

In principle, the sum over m in Eqs. (5)–(7) includes all propagating modes and evanescent modes (imaginary k_m^{ζ}). However, in the real calculations, we take all the propagating modes and several lowest evanescent modes into account to meet the desired precision. The matching conditions are determined by the requirement of continuity of the displacement u and the stress $C_{44} \partial u/\partial x$ at the interfaces I–II and II–III

$$u^{\mathrm{I}}(x = 0, y) = u^{\mathrm{II}}(x = 0, y), \tag{8}$$

$$\left[\partial u^{\mathrm{I}}(x, y)/\partial x\right]\big|_{x=0} = \left[\partial u^{\mathrm{II}}(x, y)/\partial x\right]\big|_{x=0}, \tag{9}$$

$$u^{\mathrm{II}}(x = L, y) = u^{\mathrm{III}}(x = L, y), \tag{10}$$

$$\left[\partial u^{\mathrm{II}}(x, y)/\partial x\right]\big|_{x=L} = \left[\partial u^{\mathrm{III}}(x, y)/\partial x\right]\big|_{x=L}. \tag{11}$$

Multiplying Eq. (8) by $\phi_m^{\mathrm{I}}(y)$, Eqs. (9) and (10) by $\phi_m^{\mathrm{II}}(y)$, and Eq. (11) by $\phi_m^{\mathrm{III}}(y)$, respectively, and then integrating over y, we obtain the equations for the coefficients in Eqs. (5)–(7) required. After rewriting the resulting equations in the form of matrix, we can derive the transmission coefficient τ_m by the scattering matrix method [29–31].

3. Numerical results and discussion

To envisage the effect of the discontinuity on the thermal conductance, we begin with the study of the transmission coefficient through the structure, as depicted in Fig. 1. In the following numerical calculations, we always choose the parameters: $W_{\mathrm{I}} = 12$ nm and $L = 12$ nm, and employ the values of elastic stiffness constant and the mass density [32]: $C_{44}(\mathrm{GaAs}) = 5.99(10^{10}\ \mathrm{N\,m^{-2}})$, and $\rho(\mathrm{GaAs}) = 5317.6(\mathrm{kg\,m^{-3}})$.

We first display the dependence of the total transmission coefficients on the reduced frequency ω/Δ for different stub heights h_2 in Fig. 2. Here, $\Delta = \omega_{m+1} - \omega_m = \pi v_{\mathrm{SH}}/W_{\mathrm{I}}$ (v_{SH} is the acoustic wave velocity in structure) denotes the splitting of the cutoff frequency between the $(m+1)$th and mth modes in region I. As the stubs is absent, i.e., $h_1 = h_2 = 0$, the total transmission coefficient shown in curve a in Fig. 2(a) exhibits perfect transmission steps and an abrupt jump

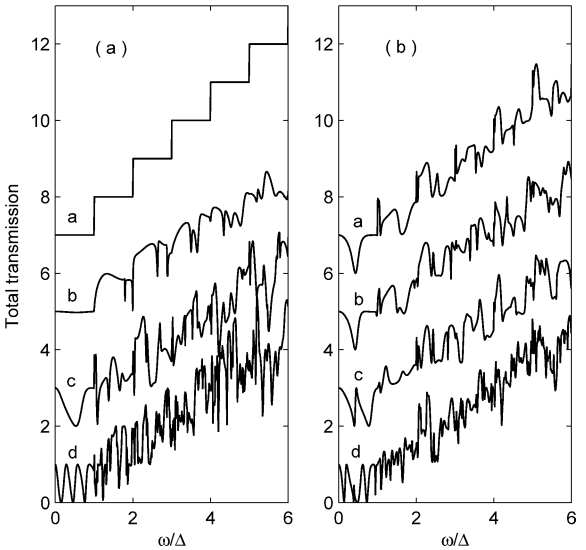

Fig. 2. Total transmission coefficient as a function of the reduced frequency ω/Δ of the incident phonons for the different heights h_2. (a) Curves a–d correspond to the different heights $h_2 = 0, 1, 12$, and 40 nm, respectively. Here $h_1 = h_2$. (b) Curves a–d correspond to the different heights $h_2 = 0, 1, 6$, and 40 nm, respectively. Here $h_1 = 12$ nm. Two consecutive curves are vertically offset by two units for clarity. Hereafter, we always choose $W_{\mathrm{I}} = 12$ nm and $L = 12$ nm in calculations.

always locates just at an integer reduced frequency. This is due to the structure becoming a continuity quantum waveguide. When h_1 and h_2 are increased to 1 nm simultaneously, the transmission plateaus are observed to resolve into a number of peak-dip structures, except the first plateau being almost unchanged. With further increase of the heights h_1 and h_2, the transmission spectra display more complex oscillation behaviors (see curves c and d in Fig. 2(a)), and the lowest plateau also resolves into a peak-dip structure. When the height h_1 is fixed (i.e., 12 nm), however, we can see from Fig. 2(b) that the total transmission coefficient exhibits rather complicated oscillation behavior ever for $h_2 = 0$, and also becomes more and more complicated with the increase of h_2. These phenomena can be well understood. Increasing the heights h_1 and/or h_2 leads to a lowering of the cutoff frequency of the propagating wave along the stubs. Thus, more modes can be excited in region II when the height of the stubs h_1 and/or h_2 are higher. These modes will interfere with each other due to the multiple reflection of the phonon waves in region II. As a result, the more complex transmission spectra are observed. Note that at $\omega \to 0$, the transmission coefficient approaches unity and is independent of the sizes of the scattering region II (i.e., L and W_{II}), unlike the case of electrical transport, where the transmission is always close to zero when the energy of the incident electron $\varepsilon_F < \varepsilon_1$ (ε_1 is the threshold energy of the lowest mode). The reason is that the stress-free boundary condition allows the propagation of the acoustic mode with $\omega \to 0$. As to why at $\omega \to 0$, the transmission coefficient is independent of the sizes of the scattering region II is due to that at $\omega \to 0$, the wavelength of the phonon is very large, and much larger than the dimension of the scattering region, the displacement field u becomes essentially the same throughout.

An interesting result in Fig. 2 is that the stop-frequency, at which all phonons are reflected completely, is clearly visible when $\omega/\Delta \leqslant 1.0$. Further calculations show that the stop-frequency only occurs when one of the heights of the stubs is equal to, or larger than the width of the main wire W_{I}, and the number of the stop-frequency increases with increasing the heights of the stubs. However, these phenomena cannot be observed in the WNW quantum structure [26]. This may be generally interpreted by the fact that the total reflection is governed by the coupling strength of the propagating lowest-order mode and the excited modes in region II. It is known that the coupling strength can be expressed by the overlap of the transverse functions of the incident wave and the excited waves: $Q_{mn} = \int \phi_m^{\mathrm{I}}(y)\phi_n^{\mathrm{II}}(y)\,dy$, where m and n are indices of the transverse modes in region I and region II, respectively. When the lowest mode 0 propagates from the narrow region I through the NWN quantum structure, more than one transverse mode can be excited in the wide region II. At this case, the overlap of the transverse functions of the incident wave and the excited waves are: $Q_{00} = \sqrt{W_{\mathrm{I}}/W_{\mathrm{II}}}$, and $Q_{0n} = \sqrt{2W_{\mathrm{II}}/W_{\mathrm{I}}}[\sin(n\pi(W_{\mathrm{I}}+h_1)/W_{\mathrm{II}}) - \sin(n\pi h_1/W_{\mathrm{II}})]/n\pi$, $(n \neq 0)$. Thus, it is possible that the total reflection occurs at certain frequencies only when W_{II} and h_1 are large enough, at which sufficient excited evanescent modes in region II interfere with the propagating lowest-order mode. In the WNW quantum structure, however, when the incident wave is only the lowest mode 0, only mode 0 can be excited in the scattering region II, and so, the overlap, $Q_{00} \neq 0$, and $Q_{0n} = 0$. This indicates that there is no coupling between the propagating lowest-order mode and the excited modes

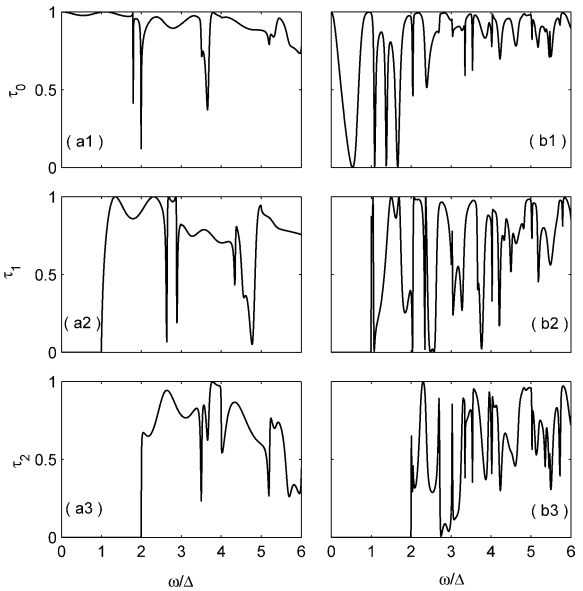

Fig. 3. Transmission coefficients for the three lowest modes as a function of ω/Δ: (a) for $h_1 = h_2 = 1$ nm, (b) for $h_1 = h_2 = 12$ nm. (a1)–(a3) and (b1)–(b3) correspond to τ_0, τ_1, and τ_2, respectively.

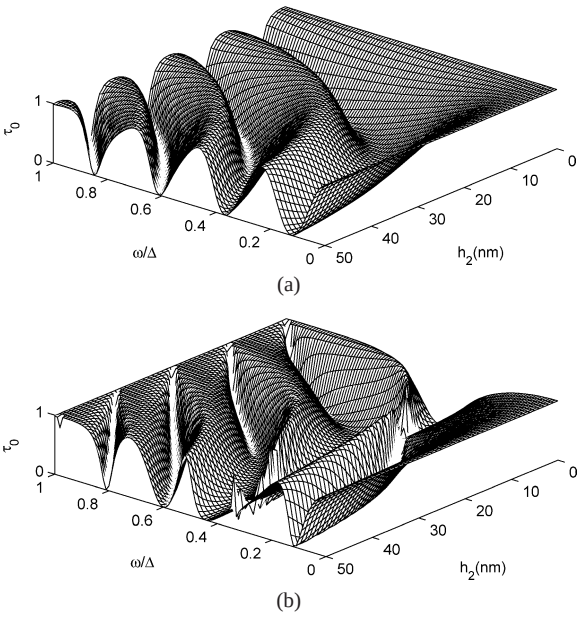

Fig. 4. Transmission coefficient versus the height h_2 and the incident phonon frequency ω/Δ, where $\Delta = \omega_{n+1} - \omega_n = \pi v_{\mathrm{SH}}/W_{\mathrm{I}}$ (v_{SH} is the acoustic wave velocity in GaAs) represents the splitting of the cutoff frequency between the $(n+1)$th mode and the nth mode in the region I. (a) for $h_1 = h_2$; (b) for $h_1 = 12$ nm.

except mode 0. As a consequence, the propagating phonons cannot be reflected totally.

In order to further reveal the transmission properties, Fig. 3 illustrates the individual modal transmission coefficients of the first three lowest modes. It is clear that for the incident modes with same index m, the transmission coefficient spectra becomes more complex as the heights h_1 and h_2 are increased simultaneously. We can also find from Fig. 3 that the threshold frequency of the onset of transmission for each mode occurs just at the corresponding integer reduced frequency ω/Δ. For the WNW quantum structure, however, the onset of transmission can be observed at the noninteger induced frequency ω/Δ, and the interval of the jumps of two consecutive modes is larger than one integer reduced frequency ω/Δ at certain parameters (see Fig. 3 in Ref. [26]). These phenomena can be understood qualitatively by taking into account that, due to different types discontinuities, the coupling of the modes in the scattering region is very different. In NWN quantum waveguide, the phonons propagate from a narrow region with very sparse modes to a wide region with dense modes. However, the reverse case is for the WNW structure. These results indicate that the different kinds of discontinuities have quite different effects on the individual modal transmission.

To show more clearly the individual modal transmission properties, we study the transmission coefficient dependence on the height h_2 and the incident phonon frequency ω/Δ for the mode 0 in the structure, as shown in Fig. 4. It is clearly observed that as $\omega \to 0$, the transmission coefficients always approach unity, and is independent of the height h_2. This indicates that the phonons are not scattered by the region II due to the presence of the stubs for incident acoustic phonon with $\omega \to 0$, as it is aforementioned. Fig. 4 also shows that the transmission coefficient exhibits a periodic pattern as a function of h_2. The periodic oscillating behavior is more clearly displayed in Fig. 5 and can be generally interpreted as follows. In region II, the propagating and reflected waves having same wavenumber, $k_m^{\mathrm{II}} = \sqrt{\omega^2/v_{\mathrm{SH}}^2 - m^2\pi^2/L^2}$, interfere with each other and form a standing wave inside the stubs. The waves reflected by the stubs will interfere with the propagating waves in the main waveguide. When the phase shift between the incident wave in the main waveguide and the reflected

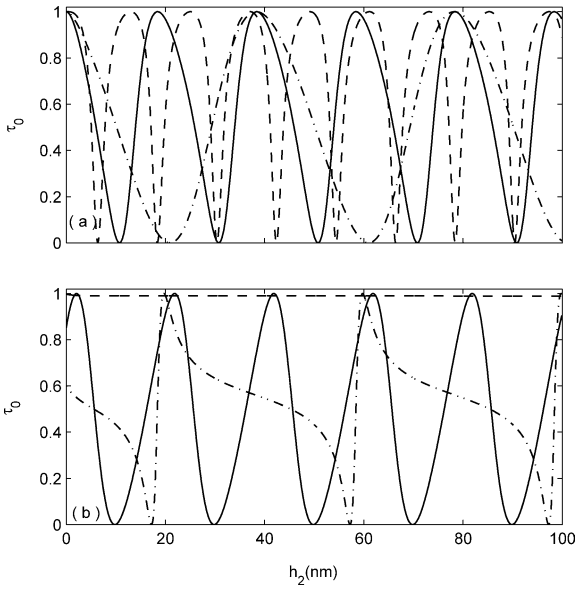

Fig. 5. Transmission coefficient as a function of the the height h_2 for different frequencies in Fig. 4: the dash-dotted, solid, and dashed curves in (a) and (b) are for $\omega/\Delta = 0.3, 0.6$, and 1.0 in Fig. 4(a) and (b), respectively. (a) for $h_1 = h_2$; (b) for $h_1 = 12$ nm.

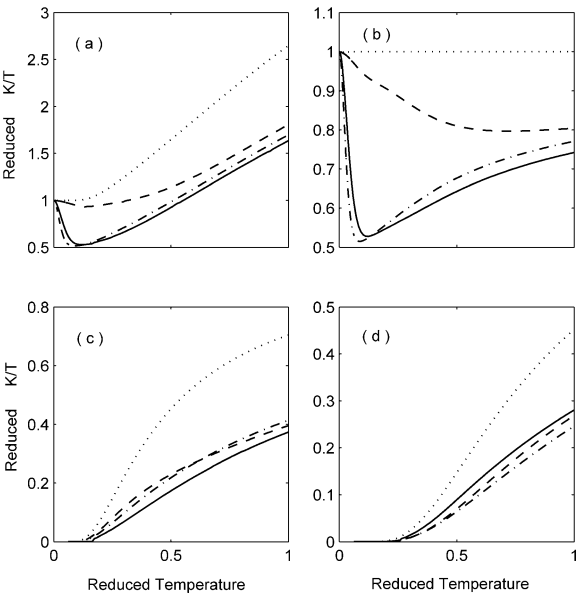

Fig. 6. Thermal conductance divided by temperature reduced by the zero-temperature universal value $\pi^2 k_B^2/3h$ as a function of the reduced temperature $k_B T/\hbar\Delta$ for the different heights h_2. (a) is for the total thermal conductance, and (b)–(d) for the thermal conductance of mode 0, 1, and 2, respectively. The dotted, dash, solid, and dashed-dotted curves correspond to $h_2 = 0, 3, 20$, and 30 nm, respectively. Here we take $h_1 = h_2$.

wave by the stubs is just equal to $2n\pi$, the transmission will be reinforced and $\tau_0 = 1$; while the phase shift is $(2n+1)\pi$, the transmission coefficient, τ_0, is zero. Consequently, a periodic oscillation appears in the transmission spectra and the period, Δh_2, of the oscillation can be obtained from $2k_0\Delta h_2 = 2\pi$, namely $\Delta h_2 = \pi/k_0 = \lambda_0/2$. Moreover, it is clearly seen from Figs. 4 and 5 that the transmission features for the case of h_1 and h_2 increasing simultaneously are very different from those for the case of h_2 being increased but h_1 fixed. These results may be helpful for the design of phonon devices.

Next, we turn to investigate the influence of the discontinuity on the thermal conductance. Fig. 6 shows the thermal conductance divided by temperature reduced by the zero-temperature universal $\pi^2 k_B^2/3h$ as a function of the reduced temperature $k_B T/\hbar\Delta_{\mathrm{SH}}$ for different heights h_2. Fig. 6(a) is for the total thermal conductance, and Fig. 6(b)–(d) correspond to the reduced thermal conductance of mode 0, 1, and 2, respectively. It should be pointed out that the total thermal conductance is the summation of the thermal conductance of the first six modes. It can be clearly seen from Fig. 6(a) that at the temperature $T \to 0$ where only the lowest mode ($m = 0$) is excited, the value of thermal conductance, K/T, approaches the ideal universal value, $\pi^2 k_B^2/3h$, and is independent of the heights of the stubs. We emphasize, again, that at the $T \to 0$, the wavelength of the incident phonons is much larger than the dimensions of the region II, the scattering of phonons by the stubs is negligible. For a continuity waveguide (i.e., $h_1 = h_2 = 0$), a thermal conductance plateau appears at low temperatures due to no scattering(see Fig. 6(a)). With an increase of temperature, T, the plateau terminates and the value of K/T linearly increases. This is because the higher transverse modes ($m > 0$) are excited and contribute to the thermal conductance at higher temperatures (as shown in Fig. 6(c) and (d)). This accords with the fact that at a higher temperature the energy contributed by each mode is given by classical equipartition and the two-dimensional heat cavity is proportional to T^2, and so the value of $K/T \propto T$. When the stubs exist, we can find from Fig. 6(a) that the reduced total thermal conductance decreases from the universal value to a minimum at low temperatures, then increases gradually with increasing temperature. From Fig. 6(b), we

find that the reduced thermal conductance of mode 0 is a constant for the continuity waveguide, and the change is same as that of the total thermal conductance when the heights of the stubs increase. The upturn in the reduced thermal conductance of mode 0, K/T, arises from the reduced scattering as the wave vectors of mode 0 increase with temperature [19]. On the contrary, the reduced thermal conductance of the higher modes (i.e., $m = 1, 2, 3, \ldots$) increases monotonically with temperatures (see Fig. 6(c) and (d)). Thus, the scattering of the mode 0 is responsible for the decreasing of the reduced total thermal conductance K/T, but the subsequent increase is due to the combined effect of the mode 0 and thermal excitation of the higher modes. Moreover, we find from Fig. 6(b)–(d) that the reduced thermal conductance K/T decreases with the increase of the index m. By calculation it is found that the reduced thermal conductance of mode 6 is very small over the whole temperature range examined. Therefore, we take the summation of the thermal conductance of the first six modes as the total thermal conductance.

It is also obvious from Fig. 6(a) and (b) that with an increase of h_1 and h_2 simultaneously, both the reduced total thermal conductance and the reduced thermal conductance of mode 0, K/T, shift down, and the change is more sensitive to the smaller h_2. At higher temperatures (> 0.14), however, a reverse case occurs where the reduced thermal conductance is increased with increasing h_2 when the height $h_2 > 20$ nm. Further calculations show that when $h_2 > 30$ nm, the variation of the reduced thermal conductance is very small. From Fig. 6(c), we find that with the increase of h_2 and h_1, the value K/T of mode 1 decreases first, and reaches a minimum when $h_2 = h_1 = 20$ nm, then increases until $h_2 > 30$ nm. However, the dependence of the reduced thermal conductance of mode 2 on h_1 and h_2 is rather complicated: the value K/T varies between the values $h_2 = h_1 = 20$ and 30 nm. These results indicate that the temperature dependence of the thermal conductance of different modes is very different due to the different coupling strength between the incident modes and the scattering modes for different indexes of the modes and temperature. The striking feature in Fig. 6 is that when the stubs exist, the values of the total and individual thermal conductances are much less than that in the continuity case, indicating that the scattering is important

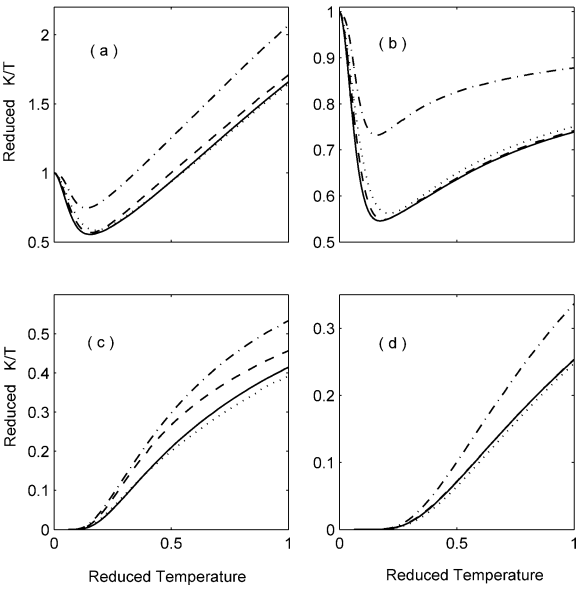

Fig. 7. Thermal conductance divided by temperature reduced by the zero-temperature universal value $\pi^2 k_B^2/3h$ as a function of the reduced temperature $k_B T/\hbar\Delta$ for the different heights h_2. (a) is for the total thermal conductance, and (b)–(d) for the thermal conductance of mode 0, 1, and 2, respectively. The dash-dotted, dotted, dashed, and solid curves correspond to $h_2 = 0, 9, 12$, and 15 nm, respectively. Here we take $h_1 = 12$ nm. Note that the dashed and solid curves in (d) are almost superposed.

over the whole reduced temperature range examined (< 1.0). These results originate from the significant reduction of the total transmission coefficient due to strong scattering of phonons by the stubs, as shown in Fig. 2.

When fix $h_1 = 12$ nm, there is no thermal conductance plateau, even for $h_2 = 0$, as shown in Fig. 7(a). At low temperatures (< 0.2), the reduced total thermal conductance decreases with increasing h_2, and the change becomes more and more slower as the height h_2 is increased. When the reduced temperature is higher (> 0.2), at small height, $h_2 \leqslant 9$ nm, the conductance decreases due to the reduction of the phonons transmission with increasing h_2. At intermediate height, $9 < h_2 \leqslant 12$ nm, the conductance increases as the height h_2 is increased. With a further increasing of the height h_2, the conductance decreases with increase of the height h_2. Further calculations show that when $h_2 > 15$ nm, the change of the total thermal conductance is very small. In order to explore these phenomena, we also present the reduced thermal

conductances of individual modes in Fig. 7(b)–(d). From Fig. 7(b), we can see that the reduced thermal conductance of mode 0 decreases with increasing h_2, and the change becomes very slow when $h_2 > 9$ nm. However, the change of the thermal conductance of mode 1 and mode 2 is same as that of the total thermal conductance, and the values at $h_2 = 12$ and 15 nm are larger than that at $h_1 = 9$ nm (see Figs. 7(c) and (d)). Thus, it is the combination of the three modes leads to the behaviors of the total K/T. From the results obtained above, it can be concluded that the variation of the thermal conductance is different for the different configurations. Therefore, we can control the heat conductance to some extent by adjusting the structural parameters.

4. Summary

We have investigated the effect of the discontinuity on the phonon transmission and thermal conductance in the narrow-wide-narrow quantum waveguide at low temperatures by employing a scattering matrix method. The total transmission coefficient versus the reduced frequency exhibits strong resonant behavior due to the presence of the discontinuity. When the height of the stub is larger than the width of the main waveguide, the stop-frequency appears. The transmission spectra will vary periodically with the height of the stub when only the zero mode is excited in the structure. At low temperatures, the reduced thermal conductance decreases from the universal quantum value at zero temperature due to the scattering of the mode 0 at the discontinuity. As the temperature increases, the thermal conductance behaves as $K/T \propto T$ since higher modes begin to play a role. The calculated results show that the total thermal conductance is also sensitive to the heights the stubs. From these results, it is believed that by designing discontinuities in dielectric quantum waveguide may provide available way to control the thermal conductance to match practical requirements in devices.

Acknowledgements

This work was supported by the National Natural Science Foundation of China, and by the Chinese Academy of Science.

References

[1] G. Chen, Int. J. Therm. Sci. 39 (2000) 471;
G. Chen, Microscale Thermophys. Eng. 5 (2001) 71.
[2] D.G. Cahill, W.K. Ford, K.E. Goodson, et al., J. Appl. Phys. 93 (2003) 793.
[3] Y.S. Ju, K.E. Goodson, Appl. Phys. Lett. 74 (1999) 3005.
[4] D. Song, G. Chen, Appl. Phys. Lett. 84 (2004) 687.
[5] A. Balandin, K.L. Wang, Phys. Rev. B 58 (1998) 1544.
[6] M.V. Simkin, G.D. Mahan, Phys. Rev. Lett. 84 (2000) 927.
[7] S.T. Huxtable, A.R. Abramson, C.L. Tien, et al., Appl. Phys. Lett. 80 (2002) 1737.
[8] S.G. Volz, G. Chen, Appl. Phys. Lett. 75 (1999) 2056.
[9] J. Zou, A. Balandin, J. Appl. Phys. 89 (2001) 2932.
[10] N. Mingo, L. Yang, D.Y. Li, A. Majumdar, Nano Lett. 3 (2003) 1713;
N. Mingo, L. Yang, D.Y. Li, A. Majumdar, Phys. Rev. B 68 (2003) 113308.
[11] D.M. Leitner, Phys. Rev. B 64 (2001) 094201.
[12] P. Kim, L. Shi, A. Majumdar, P.L. McEuen, Phys. Rev. Lett. 87 (2001) 215502.
[13] N.G. Mensah, G. Nkrumah, S.Y. Mensah, F.K.A. Allotey, Phys. Lett. A 329 (2004) 369.
[14] D.J. Yang, S.G. Wang, Q. Zhang, P.J. Sellin, G. Chen, Phys. Lett. A 329 (2004) 207.
[15] D.E. Angelescu, M.C. Cross, M.L. Roukes, Superlattices Microstruct. 23 (1998) 673.
[16] L.G.C. Rego, G. Kirczenow, Phys. Rev. Lett. 81 (1998) 232;
L.G.C. Rego, G. Kirczenow, Phys. Rev. B 59 (1999) 13080.
[17] M.P. Blencowe, Phys. Rev. B 59 (1999) 4992.
[18] K. Schwab, E.A. Henriksen, J.M. Worlock, M.L. Roukes, Nature 404 (2000) 974.
[19] D.H. Santamore, M.C. Cross, Phys. Rev. B 63 (2001) 184306.
[20] D.H. Santamore, M.C. Cross, Phys. Rev. Lett. 87 (2001) 115502;
D.H. Santamore, M.C. Cross, Phys. Rev. B 66 (2002) 144302.
[21] M.C. Cross, R. Lifshitz, Phys. Rev. B 64 (2001) 085324.
[22] Q.F. Sun, P. Yang, H. Guo, Phys. Rev. Lett. 89 (2002) 175901.
[23] Y. Xiao, X.H. Yan, J.X. Cao, et al., Phys. Rev. B 69 (2004) 205415.
[24] S.X. Qu, M.R. Geller, Phys. Rev. B 70 (2004) 085414.
[25] T. Yamamoto, S. Watanabe, K. Watanabe, Phys. Rev. Lett. 92 (2004) 075502.
[26] W.-X. Li, K.-Q. Chen, W.H. Duan, J. Wu, B.L. Gu, J. Phys. D: Appl. Phys. 36 (2003) 3027.
[27] W.-X. Li, K.-Q. Chen, W.H. Duan, J. Wu, B.L. Gu, J. Phys.: Condens. Matter 16 (2004) 5049.
[28] W.-X. Li, K.-Q. Chen, W.H. Duan, J. Wu, B.L. Gu, Appl. Phys. Lett. 85 (2004) 822.
[29] H. Tamura, T. Ando, Phys. Rev. B. 44 (1991) 1792.
[30] M. Leng, C.S. Lent, Phys. Rev. Lett. 71 (1993) 137;
M. Leng, C.S. Lent, Phys. Rev. B. 50 (1994) 10823.
[31] H.Q. Xu, Phys. Rev. B. 52 (1995) 5803;
H.Q. Xu, Appl. Phys. Lett. 80 (2002) 853.
[32] O. Madelung, Semiconductors: Group IV Elements and III–V Compounds, Springer, Berlin, 1982.